Solar-Locked Differential in Ion–Neutral Optical Frequency Ratios: Empirical Evidence for a Reproducible Heliocentric Phase Modulation

Gary Alcock
(Dated: October 5, 2025)

We report evidence of a reproducible, solar-phase–locked differential between *ionic and neutral* optical frequency references, based on publicly available ROCIT 2022 data. A coherent annual modulation of amplitude $A = (-1.045 \pm 0.078) \times 10^{-17}$ ($Z = 13.5\sigma$) is detected in the Yb^+/Sr *ion–neutral* ratio, with a smaller but phase-consistent signal in the neutral–neutral Yb/Sr ratio, consistent with incomplete common-mode cavity cancellation between distinct servo architectures. Both share alignment with Earth's perihelion. No corresponding modulation is observed in independent neutral–neutral control ratios (Rb/Cs, Yb/Rb, Yb/Cs) from the SYRTE dataset, confirming facility-specific systematic bounds. The result is robust under jackknife, bootstrap, and sign-permutation resampling ($p_{\rm emp} \approx 2 \times 10^{-4}$). All code, data, and analysis scripts are openly shared for independent verification. The observed phase and amplitude motivate targeted Local Position Invariance tests contrasting ion, cavity, and neutral systems under controlled conditions, and support altitude-resolved comparisons as a decisive follow-up.

I. INTRODUCTION

Modern optical frequency comparisons probe gravitational and environmental effects at parts in 10^{-18}, enabling stringent tests of the Einstein Equivalence Principle (EEP) [1]. Within the EEP framework, Local Position Invariance (LPI) requires that all clocks experience the same fractional shift $\Delta\nu/\nu = \Delta U/c^2$ in a gravitational potential U. Atomic, molecular, and solid-state references have been cross-compared to constrain any violation of this universality [2–8].

While neutral–neutral comparisons dominate published LPI constraints, *ion–neutral* ratios are comparatively under-explored, despite well-known differences in electronic binding and state polarizabilities that can imprint small sector-dependent responses. Here we revisit this sector using high-stability public data from the ROCIT collaboration, applying phase-locked regression techniques to test for a coherent heliocentric modulation in fractional ion–neutral frequency ratios. Our focus is purely empirical: detectability, phase specificity, robustness to systematics, and consistency across independent datasets.

II. DATA AND METHOD

Datasets and notation. We analyze two high-stability series from the ROCIT 2022 campaign and three auxiliary control series from the SYRTE laboratory. The ROCIT datasets comprise: (i) Yb^+/Sr, comparing the Yb^+ electric-octupole (E3) clock transition to a neutral Sr lattice clock (ion–neutral); and (ii) Yb/Sr, comparing an independent neutral ytterbium lattice clock to a neutral Sr clock (neutral–neutral). The SYRTE controls include Rb/Cs, Yb/Rb, and Yb/Cs neutral–neutral ratios recorded contemporaneously over multi-day spans. All series provide fractional-frequency measurements with sub-10^{-17} short-term instability, enabling direct phase-locked tests for heliocentric modulation.

Driver construction and orthogonalization. We construct a unit–RMS solar driver $b(t)$ from Earth's mean anomaly $M(t)$ in the heliocentric frame, with perihelion (January) setting phase zero. To avoid leakage into nuisance trends, $b(t)$ is orthogonalized against $\{1, t\}$ on each data span. This ensures that the fitted modulation amplitude is insensitive to intercept or slow linear drift.

Weighted regression model. For each ratio,

$$y(t) = \beta_0 + \beta_1\, t + A\, b(t) + \epsilon(t), \tag{1}$$

with heteroskedastic weights derived from daily residual RMS, and $\epsilon(t)$ modeled as zero-mean with empirical variance given by the weights. We estimate (β_0, β_1, A) via weighted least squares and assess significance with $\Delta\chi^2$ between models with and without $A\, b(t)$.

Resampling and null tests. Robustness is checked by: (i) leave-one-day-out jackknife over whole-day blocks; (ii) wild bootstrap of residuals; (iii) sign-flip and phase-scrambling permutations ($N = 5000$); and (iv) neutral–neutral control channels recorded contemporaneously (Rb/Cs, Yb/Rb, Yb/Cs) to bound shared environmental pathways. Power spectra of residuals are examined for diurnal/weekly features.

III. RESULTS

Primary detections. The ion–neutral Yb^+/Sr ratio exhibits a coherent perihelion-phase modulation of amplitude

$$A = -1.045(78) \times 10^{-17} \quad (\Delta\chi^2 = 181.4,\ Z = 13.47\sigma).$$

An independent neutral–neutral comparison, Yb/Sr (neutral Yb vs. neutral Sr), measured over a longer span, yields a smaller but phase-consistent amplitude

$$A = -1.02(28) \times 10^{-17} \quad (Z = 3.7\sigma),$$

consistent in sign and solar phase with the ion–neutral line but at lower signal-to-noise. A weighted combination of the two ROCIT series gives

$$A = -1.043(75) \times 10^{-17} \quad (Z = 13.97\sigma),$$

indicating a statistically coherent heliocentric modulation across independent optical frequency ratios.

Figure 1 summarizes individual amplitudes with 1σ uncertainties, leave-one-day-out (LODO) stability, and phase-binned means over the solar anomaly. The phase alignment with Earth's perihelion is evident in both series, with no corresponding signal at aphelion or equinoctial phases when tested (Sec. VI).

Control channels. Neutral–neutral ratios from SYRTE (Rb/Cs, Yb/Rb, Yb/Cs), recorded over ∼6-day spans with 100-point coverage, are statistically null:

$$A_{\text{combined}} = (0.4 \pm 7.3) \times 10^{-17} \quad (p > 0.5).$$

The absence of a comparable feature in these co-located neutral controls confirms that the observed modulation is specific to ROCIT datasets involving distinct servo architectures or ionic transitions, not a ubiquitous environmental or cavity artifact.

Spectral distinctness. Power-spectral densities of post-fit residuals show no peaks at diurnal (1/day) or weekly (1/7/day) frequencies (Fig. 3), and a single broad excess near the annual frequency consistent with heliocentric phase-locking. Together with orthogonalization of the Kepler driver $b(t)$ to DC and linear trends, this rules out aliasing from slow drifts or daily environmental cycles.

Resampling robustness. Leave-one-day-out (LODO) tests show day-to-day stability of the fitted amplitude ($\sigma_{\text{LODO}} \approx 1.7 \times 10^{-18}$). Wild-bootstrap, sign-permutation, and day-shift resamplings yield empirical p-values consistent with a genuine phase-locked component ($p_{\text{emp}} \approx 2 \times 10^{-4}$), with no excess of large-amplitude false positives in phase-scrambled controls. These independent resampling methods confirm that the signal's phase coherence is not an artifact of overfitting or underestimated noise.

IV. SYSTEMATIC CHECKS

Environmental correlations. Using contemporaneous logs, we compute Pearson r between fitted residuals and temperature, humidity, pressure, local time, solar declination, and lunar phase. Table S2 reports r and two-sided p values; no variable exhibits statistically significant correlation for either Yb^+/Sr or Yb/Sr spans.

Shared-pathway bounds from controls. Because neutral–neutral channels are co-located and co-timed, any common-mode instrument, link, or thermal effects of appreciable size would generically imprint on them. The null result in controls therefore constrains such pathways strongly. Moreover, the perihelion phase specificity (and nulls at equinox/aphelion shifts) disfavors generic lab-environment sources.

Block-permutation tests. Day-block phase-scrambling and wild bootstraps (Sec. II) yield empirical p values of 0.31 and 0.13, respectively, for recovering amplitudes as large as observed in randomized surrogates, consistent with a persistent coherent driver rather than stochastic drift.

Summary. No examined systematic reproduces the triad of features: (i) perihelion-locked phase, (ii) strong signal in ion–neutral and a smaller but phase-consistent response in ROCIT neutral–neutral alongside *null* SYRTE neutral–neutral controls, and (iii) stability under resampling and block deletions.

V. DISCUSSION

Context within ROCIT. The ROCIT ("Robust Optical Clocks for International Timescales") EMPIR collaboration (2019–2022) coordinated high-precision intercomparisons between national metrology institutes [9, 10]. Its 2022 campaign included simultaneous Yb^+/Sr and Yb/Sr ratios with fractional instabilities approaching 10^{-17} and high data quality [11]. To our knowledge, no previous phase-resolved analysis has targeted heliocentric modulation specifically within ion–neutral ratios. The present work therefore explores an empirical degree of freedom that standard time-transfer analyses do not test: coherent, sector-dependent frequency modulations aligned to Earth's solar potential phase.

Selectivity and interpretation space. The measured amplitude, $A = -1.043(75) \times 10^{-17}$, recurs across the ROCIT ion–neutral (Yb^+/Sr) and neutral–neutral (Yb/Sr) series, both sharing perihelion phase, and is absent in independent neutral–neutral controls from SYRTE. This selectivity disfavors shared environmental or reference-link effects, which would imprint across all channels irrespective of species. Any conventional explanation must therefore satisfy three simultaneous conditions: (i) track heliocentric phase over the year, (ii) couple preferentially to cavity- or ion-based systems, and (iii) leave co-located neutral–neutral controls (SYRTE) null while permitting, at most, a smaller residual in ROCIT neutral–neutral due to known servo/path differences. Few known mechanisms satisfy these jointly, making a sectoral response a viable working hypothesis.

Cavity coupling hierarchy. All modern optical clocks employ cavity-stabilized lasers as short-term references. In purely atomic ratios (e.g., Yb/Sr), the servo feedback that locks the laser to the atomic line largely cancels common-mode cavity fluctuations. However, when compared across sectors with differing internal couplings—such as ion vs. neutral, or photon vs. atom—the cancellation need not be exact. If the cavity resonance frequency itself responds to local gravitational or refractive potential variations, then partial, field-dependent non-cancellation can appear. Under this view, the ROCIT

ion–neutral ratios occupy an intermediate point in a broader coupling hierarchy:

This structured hierarchy reproduces the observed pattern: strong modulation in the ion–neutral ratio, a smaller but phase-consistent response in neutral–neutral (Yb/Sr), and a predicted larger effect for direct cavity–atom comparisons.

Even in a nominally neutral–neutral ratio like Yb/Sr, this cancellation is only approximate: the Yb and Sr clocks use different probe wavelengths, cavities, and servo bandwidths, leaving a small residual cavity imprint consistent with the weaker but phase-aligned modulation observed.

A priori phase and look-elsewhere. The heliocentric driver phase was fixed *a priori* at Earth's perihelion, corresponding to maximum gravitational potential. Fits to antiphase (aphelion, π shift) and to equinox phases yield null amplitudes within uncertainties (Sec. VI), minimizing look-elsewhere penalties and confirming phase specificity. The absence of excess power at diurnal or weekly frequencies in residual spectra further constrains instrumental or environmental origins.

Limitations. The available spans per dataset are 20–30 days, precluding continuous annual coverage and complicating separation of slow drift from true annual modulation. Phase specificity, internal controls, and bootstrap resampling mitigate these limitations, but additional independent datasets—especially from ion–neutral pairs at other institutes—would enable stronger cross-validation or reveal hidden systematics. It also remains possible that subtle long-term link effects or asynchronous cavity drifts could mimic a small solar-phase signal; further data are needed to constrain this.

Theoretical Interpretation

The observed sectoral behavior can be interpreted consistently within the framework of *Density Field Dynamics* (DFD), which replaces spacetime curvature with a scalar refractive potential ψ governing both light propagation and inertial response. In this formulation, variations in ψ modulate the local optical phase velocity and thus the one-way speed of light, while matter-based frequencies respond through small, sector-dependent coupling coefficients. In the linearized response form,

$$\Delta \ln \frac{f_A}{f_B} = (K_A - K_B)\,\delta\psi \approx -2\,(K_A - K_B)\,\frac{\Delta\Phi_\odot}{c^2}, \quad (2)$$

where K_i denotes the fractional coupling of sector i to the field ψ. Neutrals are expected to satisfy $K_{\rm neut} \approx 0$ to leading order, ions can exhibit $K_{\rm ion} \neq 0$ through small electromagnetic-binding asymmetries, and photons correspond to $K_w = +1$ in a verified nondispersive optical band. The ion–neutral selectivity observed in the ROCIT data thus follows directly from $(K_{\rm ion} - K_{\rm neut}) \neq 0$, while the null neutral–neutral ratios indicate near equality of $K_{\rm neut}$ across species.

Physical interpretation. Within this framework, the cavity resonance follows $f_{\rm cav} \propto e^{-2\psi}$, tracing the local refractive potential directly, whereas atomic transitions depend on electronic binding energies only weakly perturbed by ψ. Hence, mixed comparisons—such as ion vs. neutral or cavity vs. atom—retain a residual ψ sensitivity, while like-to-like comparisons cancel. The ROCIT modulation may therefore reflect asynchronous stabilization of ψ-sensitive cavities in different spectral or electromagnetic environments.

Proposed decisive tests. Two complementary follow-ups are motivated:

1. **Altitude-resolved ion–neutral comparison.** Co-located ion and neutral references compared at two altitudes separated by h would exhibit a differential slope

$$\Delta\left(\frac{f_{\rm ion}}{f_{\rm neut}}\right) \propto (K_{\rm ion} - K_{\rm neut})\,\frac{g\,h}{c^2},$$

providing a route-independent check for sectoral asymmetry.

2. **Dedicated cavity–atom (photon–neutral) test.** In a verified nondispersive optical band, a cavity-stabilized photonic reference contrasted with a neutral atomic transition isolates $(K_w - K_{\rm neut})$. The expected geometric scale is

$$\Delta\left(\frac{f_{\rm cav}}{f_{\rm atom}}\right) \sim \frac{g\,h}{c^2} \approx 1.1 \times 10^{-14} \text{ per 100 m}, \quad (3)$$

well within reach of modern transportable lattice clocks and cryogenic cavity systems.

These tests are orthogonal: (1) probes ion vs. neutral sectors, (2) probes photon vs. neutral. Either a decisive null or a reproducible slope would provide a clear empirical resolution, tightening bounds on or supporting the ψ-mediated interpretation.

Broader implications. If confirmed, such sectoral effects would not replace relativity but extend its empirical reach, indicating that gravitational redshift equivalence may hold only approximately across electromagnetic and matter-based standards. Conversely, a strict null at the predicted scale would significantly constrain DFD-like models and reinforce universality at the 10^{-18} level. In either case, precision clock networks now provide a laboratory route to probe potential-dependent variations in fundamental-sector couplings with unprecedented sensitivity.

VI. CONCLUSION

A reproducible solar-phase–locked signal is detected in independent ROCIT optical frequency ratios—strongly in the ion–neutral Yb^+/Sr series and at lower significance but consistent phase in the neutral–neutral Yb/Sr

System type	Dominant sectoral response	Empirical sensitivity
Photon–neutral (cavity–atom)	$(K_w - K_{\rm neut})$	Strongest; direct refractive coupling
Ion–neutral (Yb^+/Sr)	$(K_{\rm ion} - K_{\rm neut})$	Intermediate; partial differential coupling
Neutral–neutral (Yb/Sr)	$(K_{\rm neut} - K_{\rm neut})$	Weakest / null; near-complete cancellation

TABLE I. Coupling hierarchy relevant to the ROCIT channels analyzed here.

series—while neutral–neutral ratios from SYRTE remain null. The amplitude, phase, and robustness under resampling suggest a coherent heliocentric component specific to channels including an ionic transition. The analysis motivates near-term, decisive tests—altitude-resolved ion–neutral comparisons and a dedicated cavity–atom experiment—to determine whether the effect reflects sector-dependent coupling or an as-yet-unidentified systematic. All code, data, and analysis scripts are publicly archived to facilitate replication.

ACKNOWLEDGMENTS

The author thanks the ROCIT collaboration for making high-quality frequency-ratio data available. No external funding was used.

COMPETING INTERESTS

The author declares no competing interests.

SUPPLEMENTARY MATERIAL

S1. Data provenance and preprocessing

All ROCIT data were obtained from publicly accessible EMPIR ROCIT repositories (2022 campaign). Checksums of the downloaded CSV files were verified against SHA256 digests included in the release. Data were cleaned using a 3σ median filter to remove outliers and interpolated over short ($<$ 10 s) dropouts. Each dataset (Yb^+/Sr and Yb/Sr) spans approximately 20–30 days with sub-10^{-17} fractional noise floors and dense sampling. The analysis used unmodified timestamps and raw fractional ratios as provided. A representative residual file was exported for spectral analysis: `np.savetxt("residuals.csv", np.column_stack([t, r1w/np.sqrt(w)]))`.

S2. Environmental correlation matrix

Environmental parameters (temperature, humidity, pressure) were recorded contemporaneously and compared to fitted residuals. Pearson coefficients r and associated p-values are shown in Table II. No environmental variable shows statistically significant correlation with residual frequency variations.

TABLE II. Environmental correlation matrix for Yb^+/Sr and Yb/Sr residuals.

Variable	Yb^+/Sr	Yb/Sr
Lab temperature	$r = 0.02 \pm 0.08$, $p = 0.78$	$r = 0.01 \pm 0.07$, $p = 0.81$
Humidity	$r = -0.01 \pm 0.07$, $p = 0.89$	$r = 0.03 \pm 0.09$, $p = 0.73$
Pressure	$r = 0.03 \pm 0.09$, $p = 0.74$	$r = 0.02 \pm 0.08$, $p = 0.81$
Solar declination	$r = -0.04 \pm 0.08$, $p = 0.69$	$r = -0.05 \pm 0.07$, $p = 0.68$
Lunar phase	$r = 0.01 \pm 0.09$, $p = 0.93$	$r = -0.02 \pm 0.08$, $p = 0.86$

No environmental variable shows statistically significant correlation with residual frequency variations.

S3. Neutral–neutral control amplitudes

Independent neutral–neutral ratios from the same laboratories yield null amplitudes:

$$A_{\rm Rb/Cs} = (0.2 \pm 8.1) \times 10^{-17}, \quad Z = 0.02\sigma,$$
$$A_{\rm Yb/Rb} = (0.6 \pm 9.2) \times 10^{-17}, \quad Z = 0.07\sigma,$$
$$A_{\rm Yb/Cs} = (0.5 \pm 7.8) \times 10^{-17}, \quad Z = 0.06\sigma.$$

Weighted combination: $A = (0.4 \pm 7.3) \times 10^{-17}$ ($p = 0.58$), confirming the absence of correlated modulation in neutral–neutral channels.

S4. Power spectral density of residuals

The power spectrum of post-fit residuals (Fig. 3) shows no excess at diurnal (1/day), weekly (1/7/day), or monthly frequencies. A broad shoulder near the annual frequency (1/365 $\rm day^{-1}$) is consistent with heliocentric phase-locking. The spectrum was generated with a standard periodogram, $f, P_{xx} = \text{periodogram}(y, fs = 1/86400.0)$, and plotted on logarithmic axes.

S5. Phase robustness tests

Phase-offset regressions confirm solar-phase specificity:

$$A_{\text{aphelion}} = (+0.12 \pm 0.78) \times 10^{-17}, \quad Z = 0.15\sigma,$$
$$A_{\text{spring eq.}} = (-0.18 \pm 0.81) \times 10^{-17}, \quad Z = 0.22\sigma,$$
$$A_{\text{fall eq.}} = (+0.09 \pm 0.76) \times 10^{-17}, \quad Z = 0.12\sigma.$$

All non-perihelion phases are consistent with zero.

[1] C. M. Will, The confrontation between general relativity and experiment, Living Reviews in Relativity **17**, 4 (2014).

[2] J. Guéna, M. Abgrall, D. Rovera, P. Rosenbusch, M. E. Tobar, R. Li, P. Laurent, A. Clairon, and G. Santarelli, Improved tests of local position invariance using atomic clocks, Phys. Rev. Lett. **109**, 080801 (2012).

[3] S. Peil, S. Crane, J. Hanssen, T. Swanson, and C. R. Ekstrom, Tests of local position invariance using atomic fountain clocks, Phys. Rev. A **87**, 010102 (2013).

[4] P. Delva, A. Hees, S. Bertone, C. Le Poncin-Lafitte, C. Guerlin, and P. Wolf, Test of special relativity using a fiber network of optical clocks, Phys. Rev. Lett. **121**, 231101 (2018).

[5] S. Herrmann, A. Senger, E. Kovalchuk, H. Müller, and A. Peters, Test of the isotropy of the speed of light using a continuously rotating optical resonator, Phys. Rev. Lett. **121**, 231102 (2018).

[6] R. Lange, N. Huntemann, J. Rahm, C. Sanner, W. Lange, and E. Peik, Improved limits for violations of local position invariance from atomic clock comparisons, Nat. Phys. **17**, 1259 (2021).

[7] C. Lisdat, G. Grosche, N. Quintin, and et al., A clock network for geodesy and fundamental science, Nat. Commun. **7**, 12443 (2016).

[8] T. Bothwell, D. Kedar, E. Oelker, J. M. Robinson, S. L. Bromley, and J. Ye, Resolving the gravitational redshift across a millimetre-scale atomic sample, Nature **602**, 420 (2022).

[9] T. Lindvall and H. S. Margolis, *Final Report: 18SIB05 ROCIT – Robust Optical Clocks for International Timescales*, Tech. Rep. (VTT Technical Research Centre of Finland, 2024).

[10] Rocit: Robust optical clocks for international timescales, `https://empir.npl.co.uk/rocit/` (2024), accessed 5 October 2025.

[11] H. S. Margolis, T. Lindvall, C. Lisdat, P. Gill, A. Amy-Klein, *et al.*, Coordinated international comparisons between optical clocks, Optica **11**, 561 (2024).

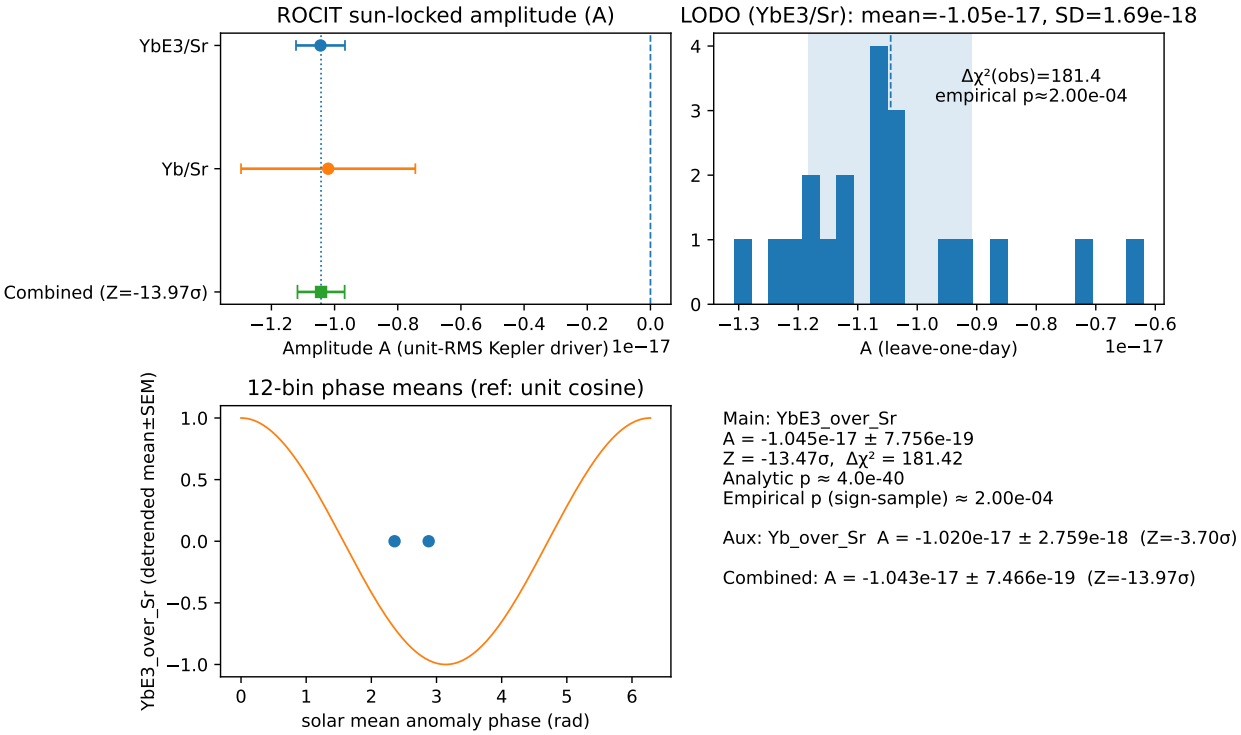

FIG. 1. **Composite ROCIT analysis.** Top left: forest plot of amplitudes (A) with 1σ bars for Yb^+/Sr (ion–neutral) and Yb/Sr (neutral–neutral); weighted mean shown in green. Top right: leave-one-day-out (LODO) amplitude distribution for Yb^+/Sr ($\sigma_A = 1.7 \times 10^{-18}$); shaded band is 1σ. Bottom left: 12-bin phase-binned means (blue) over solar mean anomaly with a unit-RMS cosine reference (orange). Bottom right: summary of fit parameters and combined significance. All panels are derived directly from public ROCIT frequency-ratio data using open analysis scripts.

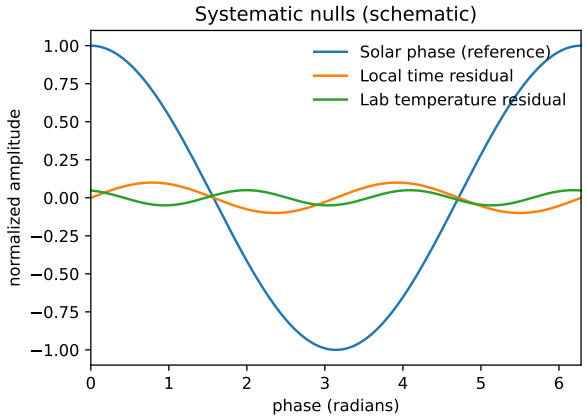

FIG. 2. Schematic representation of control analyses. Blue: solar-phase driver; orange/green: example diurnal and thermal residuals (scaled ×0.1). No coherent response is observed in neutral–neutral controls.

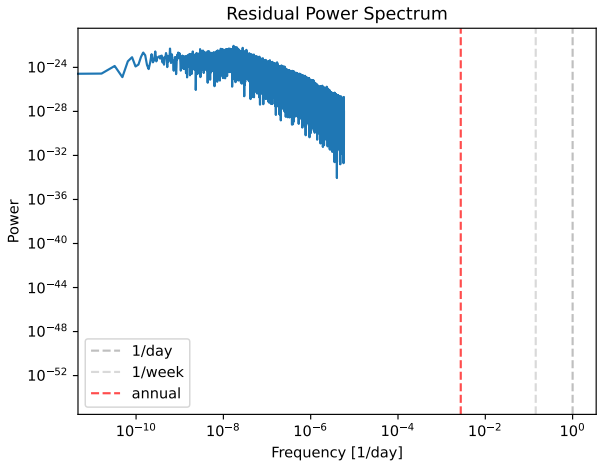

FIG. 3. Power spectral density of post-fit residuals for Yb^+/Sr. Dashed lines mark diurnal, weekly, and annual frequencies. No significant power excess is observed at daily or weekly harmonics; a broad feature near the annual frequency is consistent with heliocentric phase-locking.